4D observations of rolling contact fatigue processes by laminography using ultra-bright synchrotron radiation

Nakai, Y. ; Shiozawa, D. ; Kikuchi, S. ; Obama, T. ; Saito, H. ; Makino, T. ; Neishi, Y.

(Citation)
Engineering Fracture Mechanics,183:180-189

(Issue Date)
2017-10-01

(Resource Type)
journal article

(Version)
Accepted Manuscript

(URL)
https://hdl.handle.net/20.500.14094/90004785

4D observations of rolling contact fatigue processes by laminography using ultra-bright synchrotron radiation

Y. Nakai, D. Shiozawa, S. Kikuchi, T. Obama, H. Saito

Department of Mechanical Engineering, Kobe University, 1-1, Rokkodai, Nada, Kobe 657-8501, Japan

and

T. Makino, Y. Neishi

Research & Development, Nippon Steel & Sumitomo Metal Corporation, 1-8, Fuso, Amagasaki 660-0891, Japan

Abstract

Since rolling contact fatigue (RCF) is known to be affected by non-metallic inclusions, the RCF crack initiation and propagation mechanisms in high-strength steels were observed using ultrabright synchrotron radiation laminography. The material of the sample was a high-carbon chromium bearing steel, which intentionally contained a high concentration of sulfur to enable the observation of crack initiation from MnS inclusions. To conduct an RCF test nearby the experimental hatch of a beam line of a synchrotron radiation facility, a special RCF testing machine was developed. Fatigue tests were interrupted to conduct laminography. The fatigue life for flaking depended on the length, width, and orientation of inclusions. For every length and orientation of inclusions, vertical cracks, whose faces were perpendicular to the rolling direction, first appeared, then horizontal cracks, whose faces were parallel to the sample surface, were formed after the vertical cracks reached

a critical length. The initiation life of the vertical cracks and horizontal cracks depended on the length, width, and orientation of the MnS inclusions. The depth of horizontal crack initiation site, however, was almost independent of these parameters. The mechanism of the flaking process, which was directly observed by laminography using synchrotron radiation, was completely different from that previously supposed from observations by conventional microscopy.

1. Introduction

Bearings are generally applied under a pure rolling contact condition with oil lubrication without macroscopic slip, and rolling contact fatigue (RCF) is a crucial factor for bearings. Since non-metallic inclusions are known to have a detrimental effect on the fatigue strength of high-strength steels, the effects of the composition (chemical/mechanical properties), shape, and orientation of inclusions on RCF should be clarified and controlled.

It has been recognized that flaking starts from inclusions below the surface where the ball track is located and the shear stress is greatest, and the cracks grow from them to the surface [1, 2]. Martin et al. dealt with microstructural alterations, which develop with cyclic stressing under rolling contact, and attempted to define their nature and formation mechanisms [3]. In many cases, ‘winglike’ structural alterations, commonly called ‘butterflies’, were associated with the inclusions, as were microcracks [4-7]. Nagao et al., however, reported that the mechanism depended on the shape of the inclusions [8]. From spherical inclusions, shear-type cracks parallel to the rolling direction and surface were formed, while vertical cracks perpendicular to rolling direction were first formed from stringer-shaped inclusions. In this case, shear-type cracks were formed after the formation of vertical cracks. The formation and propagation of vertical cracks were considered to be controlled by the normal stress, while the horizontal cracks were controlled by the shear stress. Tsuchida and Tamura observed that horizontal cracks were formed from spherical inclusions, however, they considered that crack initiation was controlled by the normal stress [9].

Since these phenomena occur beneath the surface, observations have been conducted destructively by cutting samples. Thus, successive observations of RCF have not been conducted. Synchrotron radiation micro computed tomography imaging (SRCT) has been applied for the non-destructive observation of the RCF process. Stiénon et al. obtained the three dimensional (3D) shapes of non-

metallic inclusions in bearing steels by SRCT at the European Synchrotron Radiation Facility (ESRF), and calculated the stress field around them in RCF tests [10,11]. Samples exhibiting flaking damage and RCF-induced cracks were observed using SRCT by Shiozawa et al. [12] and Makino et al. [13]. In their studies, samples were cut from normal-size RCF specimens so that they included damaged areas, and the 3D imaging of the damage before flaking provided useful information on the RCF crack initiation and propagation processes. Artificial defects that simulate stringer-shaped inclusions were introduced into the specimens to investigate the effect of the shape of inclusions on crack initiation and propagation. For the successive SRCT imaging of the RCF process, samples must be sufficiently small to allow the transmission of X-rays, and the cross section must be smaller than 500 μm × 500 μm for steels. Shiozawa et al. showed that the mechanism of RCF in a thin sample is different from that in a bulk sample [14]. To investigate the effect of the shape of inclusions on crack initiation and propagation, Nakai et al. [15] employed synchrotron radiation computed laminography (SRCL) [16], which allows the high-resolution, non-destructive imaging of thin plates. In the present study, the effects of the inclusion size and orientation on RCF fatigue crack initiation and propagation are discussed based on observations obtained using SRCL.

2. Experimental procedure

2.1. Material, specimens, and RCF test

The material was the same forged high-carbon chromium bearing steel (modified JIS SUJ2) as that in a previous study [15], which intentionally contained a high concentration of sulfur to enable the observation of crack initiation from MnS inclusions, and inclusions had a preferential alignment along the forging direction as shown in Figure 1. Details of the specimen preparation procedure are given by Nakai et al. elsewhere [15]. The transverse and longitudinal cross sections of the bar corresponded to the contact surface of each specimen. The longitudinal direction of inclusions (forging direction) was either perpendicular or parallel to the specimen surface, and these inclusions were named S-type and T-type inclusions, as shown in Figures 1 (a) and (b), respectively. For the specimens with T-type inclusions, the rolling direction was selected to be perpendicular to the longitudinal direction of the inclusions.

Details of the testing machine was also given by Nakai et al. elsewhere [15]. In the present paper, results for a maximum Hertz stress, p_{max}, of 5.39 GPa are discussed. RCF tests were interrupted to conduct SRCL imaging to observe the crack initiation and propagation behaviors.

2.2. SRCL measurement setup

The SRCL imaging was carried out at an undulator beam line of the synchrotron radiation facility, SPring-8 (Super Photon Ring 8 GeV), which is set up in Hyogo, Japan. The inclination angle of the axis in the SRCL, ϕ, defined in Figure 2, was 30°, and a 37 keV monochromatic X-ray beam was employed. The experimental setup and the 3D reconstruction procedures are given Nakai et al. elsewhere [15].

3. Experimental results

3.1. S-type sample

(a) Short inclusion

An optical micrograph of a crack initiation site in a specimen with a sulfur concentration of 0.020 mass% and S-type inclusions after $N = 1.10\times10^7$ cycles (shortly after the appearance of cracks at the rolling surface) shows in Figure 3, where small cracks of length approximately 40 μm formed from an inclusion and propagated perpendicular to the ball-rolling direction. Successive observations by SRCL and RCF tests were conducted after the formation of the crack at the surface. Then, flaking was found to occur at $N_f = 1.295\times10^7$ cycles around the site where the surface crack first appeared as shown in Figure 4, where the depth of the flaking was 35 μm.

Figure 5 shows 3D images of inclusions and cracks observed by SRCL at $N = 1.10\times10^7$, 1.168×10^7, and 1.295×10^7 cycles, where (i) shows top views, (ii) shows views from the rolling direction, and (iii) shows side views of the specimen, and inclusions are indicated in pale yellow. As shown in the figure, the surface crack in Figure 3 appears to form from a stringer-shaped inclusion with a length of about 30 μm that reaches the surface, and the crack face is perpendicular to the rolling direction.

As shown in Figure 5 (a), the vertical crack had propagated further than the depth of the starter inclusion (30 μm) at $N = 1.10\times10^7$ cycles. (b) Slight growth of the crack in the depth direction was observed at $N = 1.168\times10^7$ cycles. (c) Then flaking and further growth of the vertical crack were observed at $N_f = 1.295\times10^7$ cycles. Then, the flaking is considered to occurre around the site where the vertical crack was observed. The shape at the surface observed by SRCL is similar to that observed by optical microscopy as shown in Figure 4. Since the depth of the flaking is almost the same as that of the vertical crack, the formation of the vertical crack must have affected the occurrence of the flaking although part of the vertical crack remained below the region where flaking occurred as can be seen in Figure 4 (b).

(b) Long inclusion

A surface image of a crack initiation site in a specimen with a sulfur concentration of 0.049 mass% and S-type inclusions ($N = 6.00\times10^6$ cycles, shortly after crack initiation at the surface) is shown in Figure 6. Small cracks almost perpendicular to the ball-rolling direction can be observed. After the initiation of the cracks at the surface, observation by SRCL was conducted. Flaking was found to occur at $N_f=7.67\times10^6$ cycles at the sites where the surface cracks were observed as shown in Figure 7.

3D images of inclusions and cracks observed by SRCL at $N = 6.00\times10^6$, 6.80×10^6, 7.10×10^6, 7.50×10^6, and 7.67×10^6 cycles are shown in Figure 8, where (i) shows top views, (ii) shows views from the rolling direction, and (iii) shows side views of the specimen. The inclusions at the crack initiation sites (indicated in pale yellow) are found to be longer than those shown in Figure 5. As shown in Figure 8 (a) At $N_i=6.00\times10^6$ cycles, a vertical crack formed from a stringer-shaped inclusion with a length of about 60 μm that reaches the surface, and the crack face is perpendicular to the rolling direction. (b) At $N = 6.80\times10^6$ cycles, the vertical crack propagated to the deepest point of the starter inclusion without propagation along the surface. (c) At $N = 7.10\times10^6$ cycles, a horizontal crack, which was parallel to the rolling contact surface, formed at a depth of 35 μm from the surface. From (c) $N = 7.10\times10^6$ to (d) 7.50×10^6 cycles, the vertical crack propagated in the width direction under the surface, and the horizontal crack propagated in both the width and rolling directions.

Another horizontal crack was also formed from the same inclusion. Its formation site was

shallower than that of the displayed vertical crack, but unfortunately, it could not be shown in the same figure. Such horizontal cracks were also previously observed in a specimen with an artificial hole, which simulated an inclusion [13, 14].

Figure 7 shows that the flaking occurred as a result of the propagation of the horizontal crack at $N = 7.67\times10^6$ cycles. The shape of the region of flaking observed by SRCL (Figure 8 (e)) is similar to that observed on the surface by scanning electron microscopy (SEM) shown in Figure 7 (a).

3.2. T-type sample (long inclusion)

Figure 9 (a) shows a surface image of a crack initiation site in a specimen with a sulfur concentration of 0.049 mass% and T-type inclusions ($N = 1.00\times10^6$ cycles, shortly after crack initiation at the surface). Small cracks almost perpendicular to the ball-rolling direction can be observed. Then, flaking was found to occur at $N_f = 2.95\times10^6$ cycles around the site where the surface cracks first appeared as shown in (b).

3D images of inclusions and cracks observed by SRCL at $N = 1.00\times10^6$, 1.75×10^6, 2.50×10^6, and 2.95×10^6 cycles are shown in Figure 10, where (i) shows top views, (ii) shows views from the rolling direction, and (iii) shows side views of the specimen, and inclusions are indicated in pale yellow. A vertical crack initiated from an inclusion and propagated about 25 μm in the depth direction at (a) $N_i = 1.00\times10^6$ cycles. A horizontal crack parallel to the contact surface was initiated at a depth of about 15 μm (see Figure 10 (b)). After this crack propagated in the rolling direction at (b) $N = 1.75\times10^6$ cycles, it propagated to the center of the rolling track at (c) $N = 2.50\times10^6$ cycles, leading to flaking at (d) $N_f = 2.95\times10^6$ cycles. It was also observed that the horizontal crack was initiated after the vertical crack propagated in the depth direction.

Since several cracks were initiated on the rolling track those showed different growth behavior, the shapes and sizes of inclusions in the whole rolling track were observed by SRCL before conducting RCF tests. The results are shown in Figure 11, where inclusions from which flaking occurred are indicated with an asterisk. The figure suggests that flaking occurred from the inclusions when both the length and thickness were sufficient.

4. Discussion

For the samples with the two different surfer concentrations, a vertical crack first formed, and after it reached a critical depth, a horizontal crack initiated from the vertical crack. For the specimen with a sulfur concentration of 0.020 mass% and S-type inclusions, a vertical crack formed from an inclusion whose length in the thickness direction was 30 μm, and a horizontal crack was formed after the vertical crack reached a length of 50 to 60 μm, which was similar to the initiation condition for the horizontal crack in the specimen with a sulfur concentration of 0.049 mass% and S-type inclusions. The initiation condition for the horizontal crack in the sample with T-type inclusions was also similar to that of the sample with S-type short inclusions, where the deepest point of the inclusions was shallower than the horizontal crack initiation site, and the horizontal crack initiated after the vertical crack had propagated some distance from the deepest point of the inclusions. SEM observation of the surface showed that the depth of flaking was from 20 to 40 μm in both specimens, which is similar to the depth of the horizontal crack. The depth at which the shear stress on the plane parallel to the contact surface had the greatest value was 67 μm, which was determined as 0.351a (a: contact radius given by Hertz theory for contact problems) [17], meaning that the site of horizontal crack formation was not coincident with the position where the shear stress was greatest, although the formation and propagation of the horizontal crack were controlled by the shear stress. The existence of a vertical crack may thus change the shear stress distribution.

The flaking process in RCF observed in the present study is summarized in Figure 12. (1) A crack perpendicular to the rolling surface and rolling direction forms from an inclusion that is adjacent to the rolling surface. (2) The crack propagates vertically in the depth (thickness) direction under normal stress. (3) After the vertical crack propagates to a critical depth, a horizontal crack forms, which is parallel to the rolling surface. (4) The horizontal crack propagates under the shear stress to form flakes.

In most of the previously proposed mechanisms of RCF, only a horizontal crack was considered in the discussion of the RCF process. In the present study, however, the formation of the horizontal crack was induced by a vertical crack that formed before the horizontal crack. The formation of the vertical crack was affected by the maximum size of the inclusions, which was determined by the sulfur concentration and heat treatment. The orientation of the inclusions also affected the formation

of vertical cracks. The difference in the stress concentration caused by the inclusions may be responsible for the effects of these factors [18]. The number of cycles for vertical crack initiation, horizontal crack initiation, and flaking of the 0.049S mass% samples are summarized in Table 1. Although the differences between the number of cycles to initiation of the vertical and horizontal cracks, the flaking, and the propagation of the vertical cracks, $N_{i,H}$ - $N_{i,V}$, were large, the variation of number of cycles for the propagation of the horizontal cracks, N_f - $N_{i,H}$, was small. Thus, the effect of the orientation of inclusions on the number of cycles to flaking originate from the effect of the orientation of the inclusions on vertical crack initiation and propagation along the inclusion.

Not only the orientation, but also size, shape, density, and mechanical properties of inclusions must affect the flaking mechanism. Then the findings of the present observations for stringer-type inclusions must not be generalized that remains future task.

5. Conclusions

In the present study, 4D observations of the formation and propagation of cracks in the rolling contact fatigue (RCF) tests were performed on a high-strength steel by combining a newly developed compact RCF testing machine with synchrotron radiation computed laminography (SRCL), and the effects of the inclusion size and orientation on the RCF process were examined. The following results were obtained.

(1) According to observations of the flaking process, first, a crack perpendicular to the rolling surface and rolling direction formed from an inclusion adjacent to the rolling surface. Then the crack propagated vertically in the depth direction under normal stress. After the vertical crack propagated to a critical depth, a horizontal crack formed, which was parallel to the rolling surface. Finally, the horizontal crack propagated to form flakes under shear stress.

(2) Although the differences between the number of cycles to initiation of the vertical and horizontal cracks, and the number of cycles for propagation of the vertical cracks were large, the difference in the number of cycles for propagation of the horizontal cracks was minimal. Thus, the effect of the inclusion size and orientation on the number of cycles to flaking should be responsible for the effect of these parameters on the initiation and propagation of vertical cracks along inclusions.

Acknowledgments

The synchrotron radiation experiments were performed at beam line BL46XU of SPring-8 with the approval of the Japan Synchrotron Radiation Research Institute (JASRI) under proposal numbers 2014A1562, 2014A1770, 2014B1602, 2014B1890, 2015A1668, 2015A1973, 2015B1592, and 2016A1541. The authors are grateful for the technical support of Dr. K. Kajiwara (JASRI).

References

[1] Gustaf, L, Palmgren, A, Dynamic capacity of rolling bearings. J. App. Mech., Trans. ASME, 1949;16: 165-172.

[2] Styri, H., Fatigue strength of ball bearing races and heat-treated 52100 steel specimens, Proc.ASTM, 1951; 51: 682-700.

[3] Martin, J.A., Borgese S.F., and Eberhardt, A.D., Microstructural alterations of rolling – Bearing steel undergoing cyclic stressing, J. Basic Eng., Trans. ASME, 1966; 88: 555-565.

[4] Sugino, K., Miyamoto, K.,Nagumo, M., and Aoko, K., Structural alterations of bearing steels, Trans. ISIJ, 1970; 10: 98-111.

[5] Becker, P.C., Microstructural changes around non-metallic inclusions caused by rolling-contact fatigue of ball-bearing steels, Metals Technology, 1981: 234-243.

[6] Grabulov, A., Ziese, U., Zandbergen, H.W., TEM/SEM investigation of microstructural changes within the white etching area under rolling contact fatigue and 3-D crack reconstruction by focused ion beam, Scripta Materialia, 2007; 57: 635-638.

[7] Grabulov, A., Petrov, R., Zandbergen, H.W., EBSD investigation of the crack initiation and TEM/FIB analyses of the microstructural changes around the cracks formed under Rolling Contact Fatigue (RCF), International Journal of Fatigue, 2010; 32, 576-583.

[8] Nagao, M, Hiraoka, K, Unigame, Y, Influence of nonmetallic inclusion size on rolling contact fatigue life in bearing stee, Sanyo Technical Report, 2005;12: 38-45.

[9] Tsuchida, T, Tamura, E, Mechanism of crack initiation at non-metallic inclusion under rolling contact fatigue in bearing steels, Kobe Steel Engineering Reports, 2011; 61: 62-65.

[10] Stiénon, A., Fazekas, A., Buffière, J.-Y., Vincent, A., Daguier, P., Merchi, F., A new methodology based on X-ray micro-tomography to estimate stress concentrations around inclusions in high strength steels, Materials Sci. Eng. A, Materials Science and Engineering A, 2009; 513-514: 376-383.

[11] Stienon, A., Fazekas, A., Buffiere, J.-Y., Daguier, P., Merchi, F., Vincent, A., A new methodology for predicting fatigue properties of bearing steels: From X-Ray micro-tomography and ultrasonic measurements to the bearing lives distribution, Journal of ASTM International, 2010; 7: 3, 1-14, DOI: 10.1520/JAI102532.

[12] Shiozawa, D., Nakai, Y., Fukuda, Y., Neishi, Y., Makino, T., Observation of cracks in carbon steel under contact rolling fatigue by micro CT imaging using ultra-bright synchrotron radiation, Proc. 15th Int. Conf. Exp. Mech., CD-ROM, 2012; No. 2635.

[13] Makino, T., Neishi, Y., Shiozawa, D.,Fukuda, Y., Kajiwara, K., Nakai, Y., Evaluation of rolling contact fatigue crack path in high strength steel with artificial defects, International Journal of Fatigue, 2014; 68: 168-177.

[14] Shiozawa, D., Makino, T., Neishi, Y., Nakai, Y., Observation of rolling contact fatigue cracks by laminography using ultra-bright synchrotron radiation, Procedia Materials Science, 2014; 3: 154-164.

[15] Nakai, Y., Shiozawa, D., Kikuchi, S., Sato, K., Obama, T., Makino, T., Neishi, Y, In situ observation of rolling contact fatigue cracks by laminography using ultra-bright synchrotron radiation, Frattura ed Integrità Strutturale, 2014; 34: 267-275.

[16] Gondrom, S., Zhou J., Maisl M., Reiter H., Kroning M., Arnold W., X-ray computed laminography: An approach of computed tomography for applications with limited access, Nuclear Eng. Design, 1999; 190: 141-147.

[17] Johnson, K.L., Contact Mechanics, Cambridge University Press, Cambridge, U.K., 1985; 84-104, 284-289.

[18] Makino, T., Neishi, Y., Shiozawa, D., Kikuchi, S., Okada, S., Kajiwara, K., and Nakai, Y., Effect of defect shape on rolling contact fatigue crack initiation and propagation in high strength steel, International Journal of Fatigue, 2016; 92: pp.507-516.

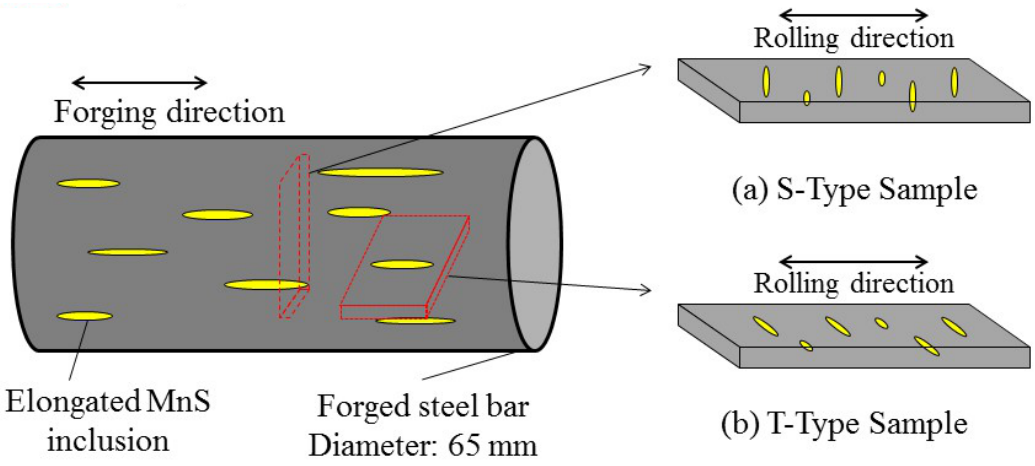

Figure 1. Orientation of inclusions in specimens.

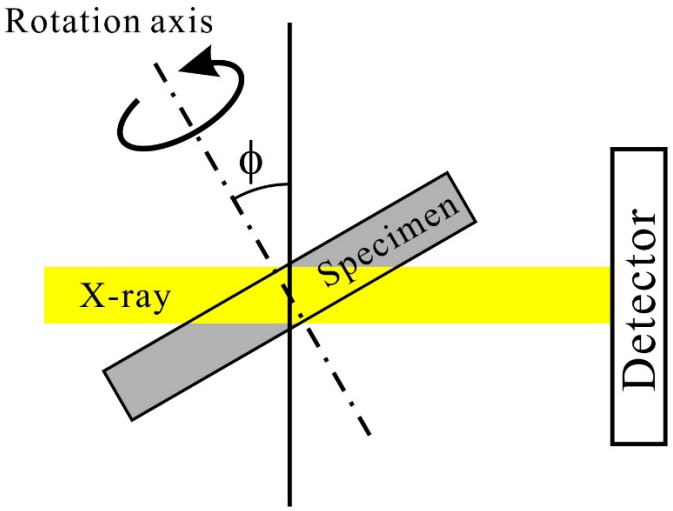

Figure 2. SRCL imaging apparatus.

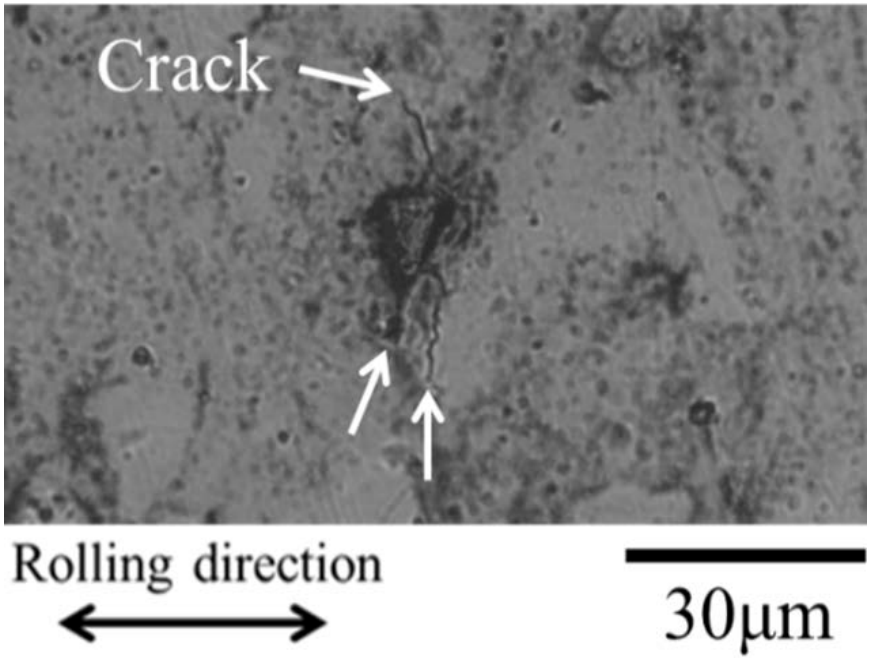

Figure 3. Optical micrograph of surface (S-type short inclusion, N_i = 1.100×10^7 cycles).

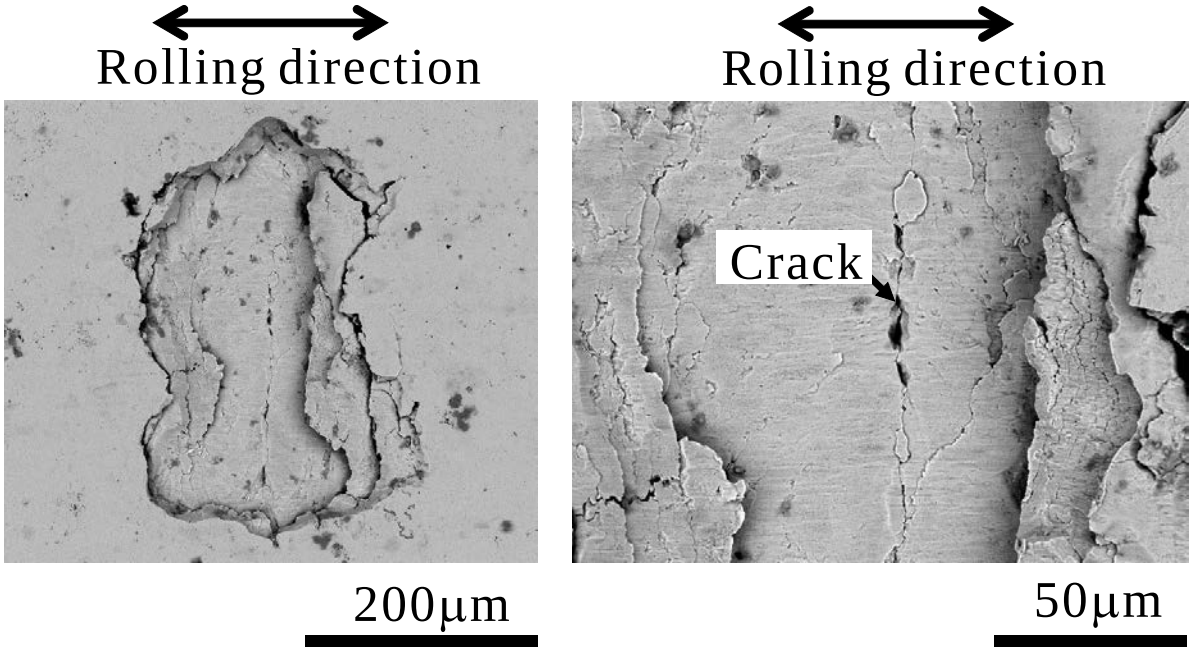

(a) Flaking (b) Enlarged view of flaking

Figure 4. SEM micrograph of surface at flaking (S-type short inclusion, N_f = 1.295×10^7 cycles).

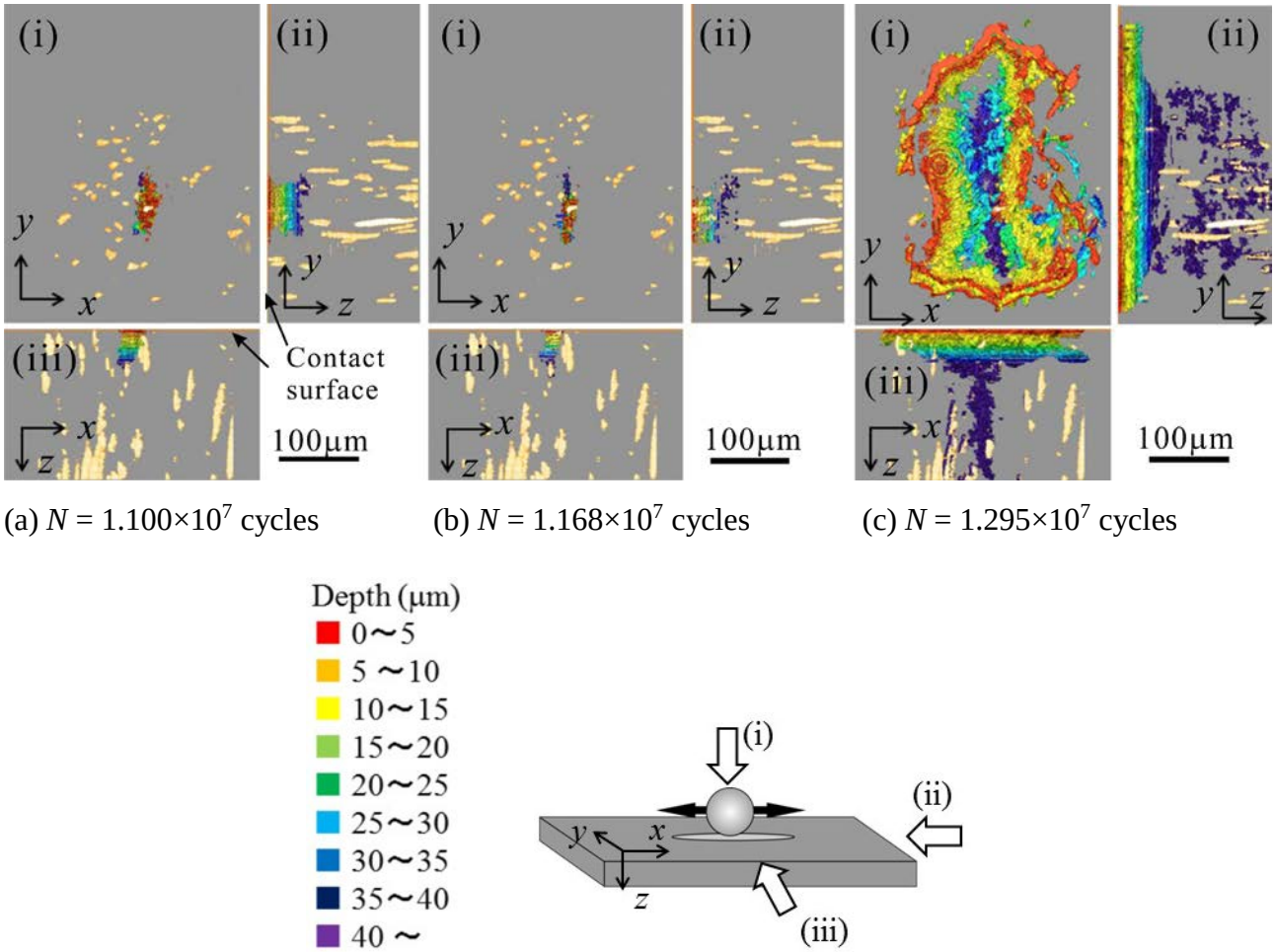

(a) $N = 1.100\times10^7$ cycles (b) $N = 1.168\times10^7$ cycles (c) $N = 1.295\times10^7$ cycles

Figure 5. 3D-images of crack and inclusion (S-type short inclusion).

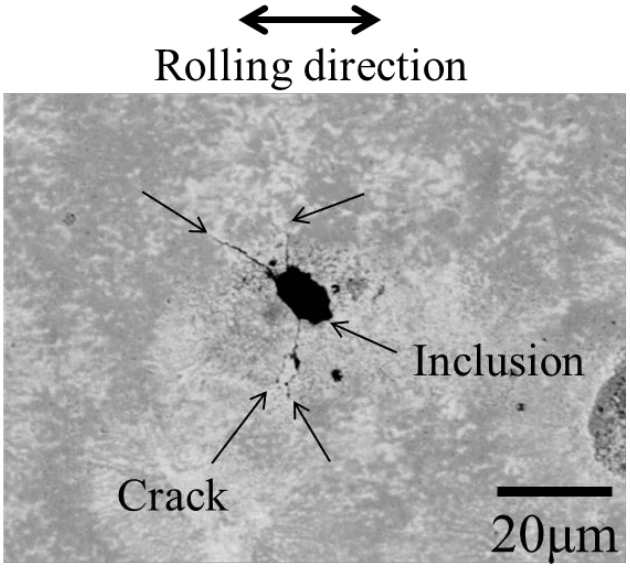

Figure 6. SEM micrograph of surface crack (S-type long inclusion, N_i = 6.00×10^6 cycles).

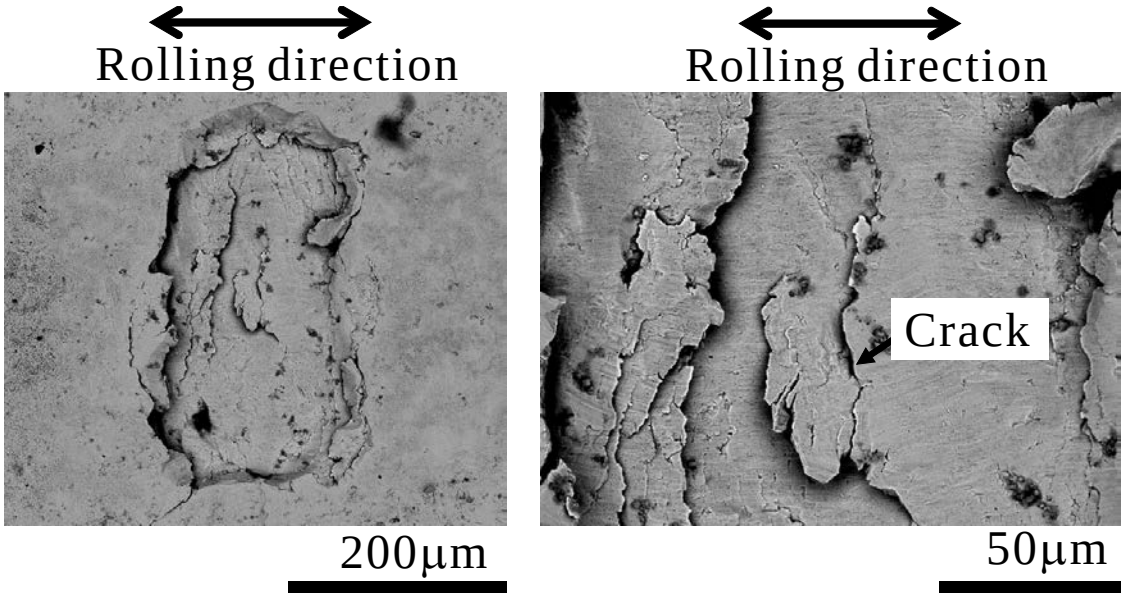

(a) Flaking (b) Enlarged view of (a)

Figure 7. SEM micrograph of surface at flaking (S-type long inclusion, N_f = 7.67×10^6 cycles).

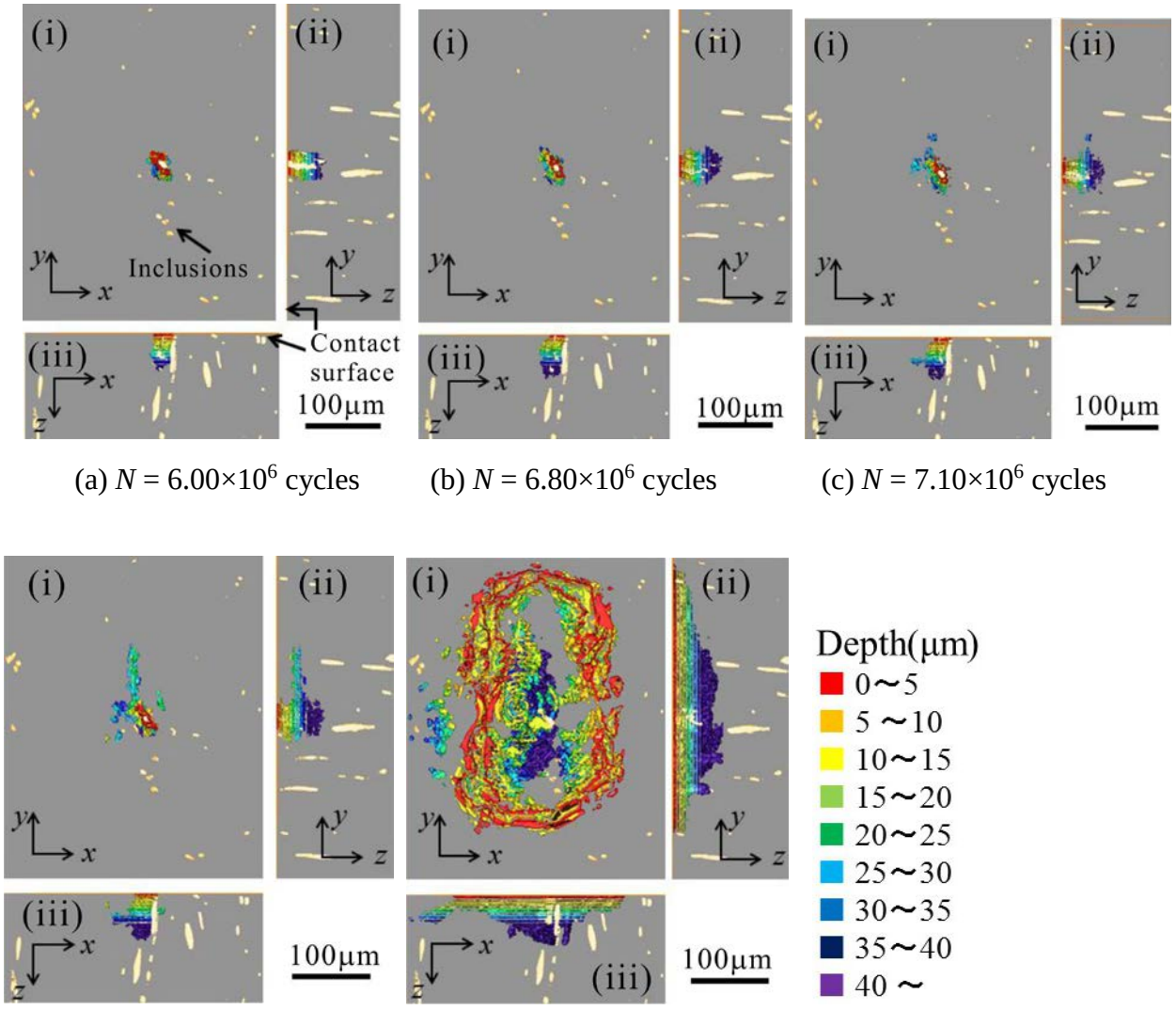

(a) N = 6.00×10^6 cycles (b) N = 6.80×10^6 cycles (c) N = 7.10×10^6 cycles

(d) N = 7.50×10^6 cycles (e) N_f = 7.67×10^6 cycles

Figure 8. 3D-images of cracks and inclusions (S-type long inclusion).

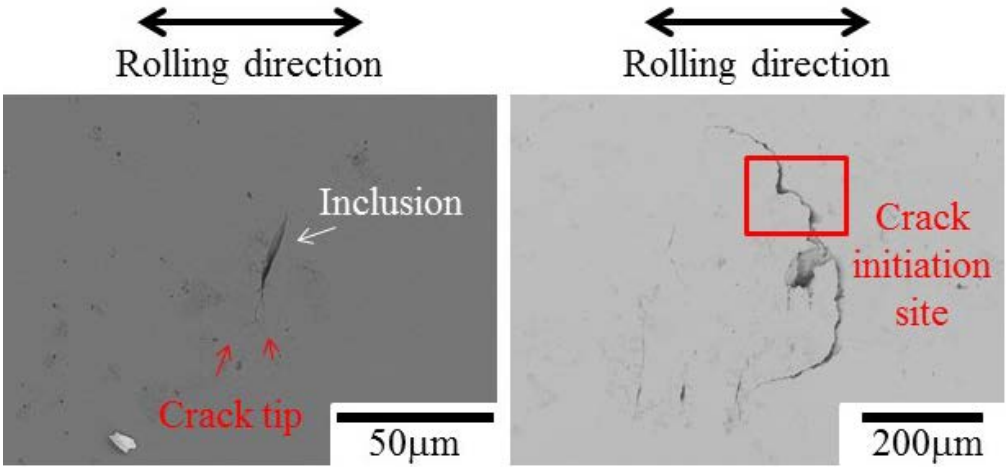

(a) N_i = 1.00×10^6 cycles (b) N_f = 2.95×10^6 cycles

Figure 9. SEM micrograph of surface crack and flaking (T-type long inclusion).

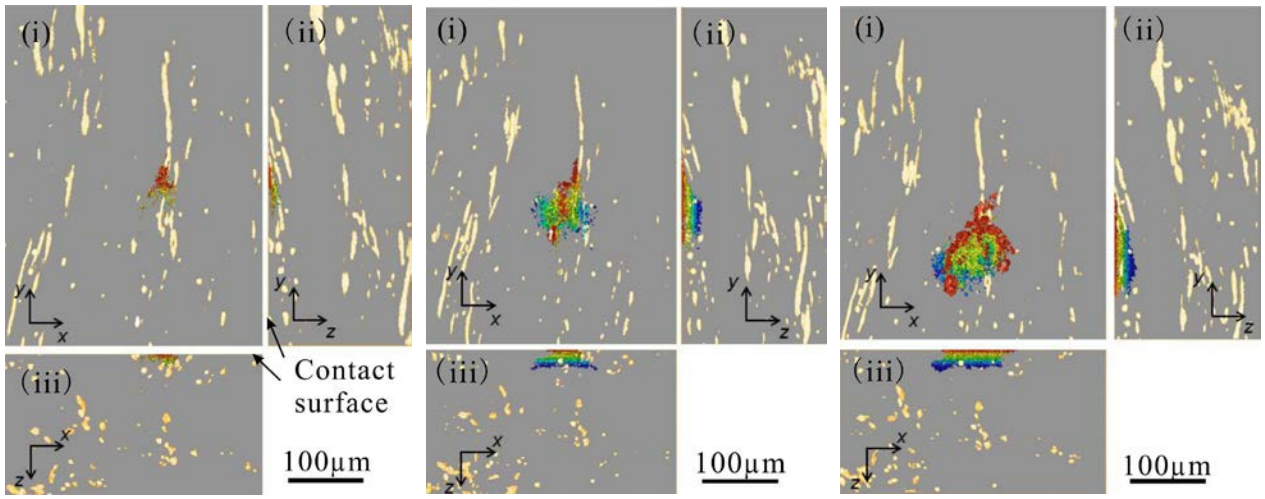

(a) N = 1.00×10^6 cycles (b) N = 1.75×10^6 cycles (c) N = 2.50×10^6 cycles

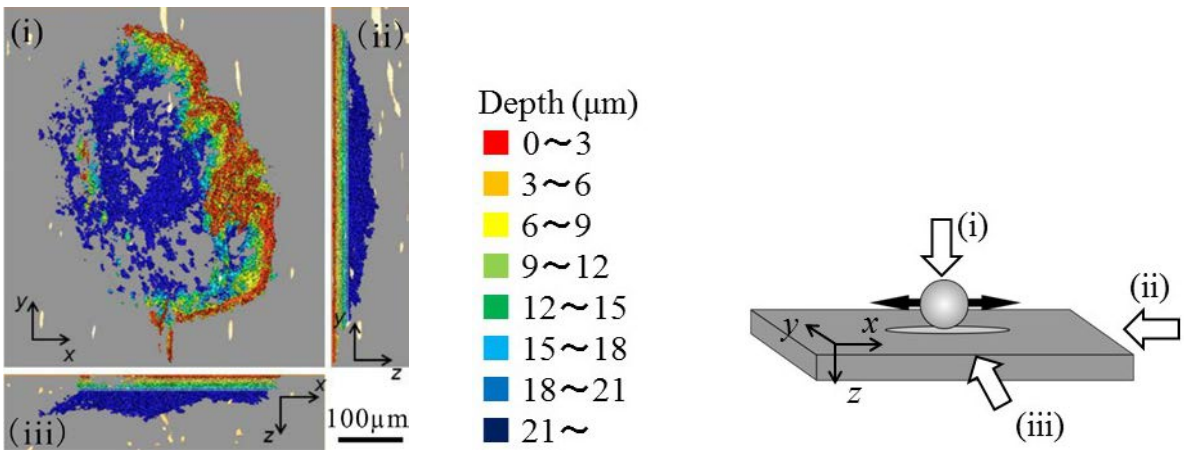

(d) N_f = 2.95×10^6 cycles

Figure 10. 3D-images of cracks and inclusions (T-type long inclusion).

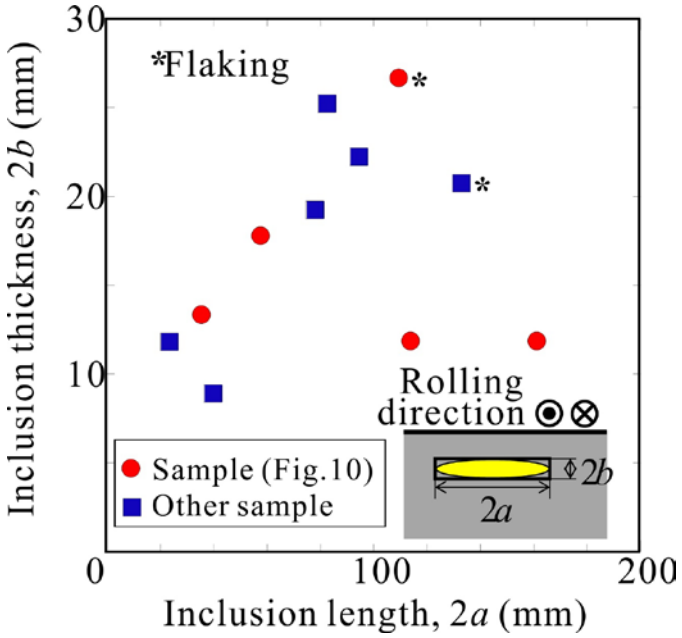

Figure 11. Relationship between thickness and length of inclusions (T-type long inclusion).

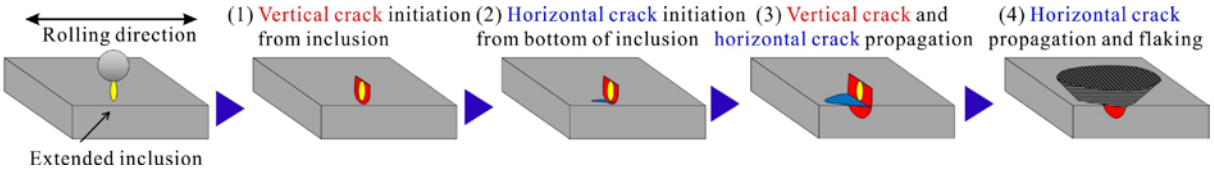

(a) S-type short inclusion.

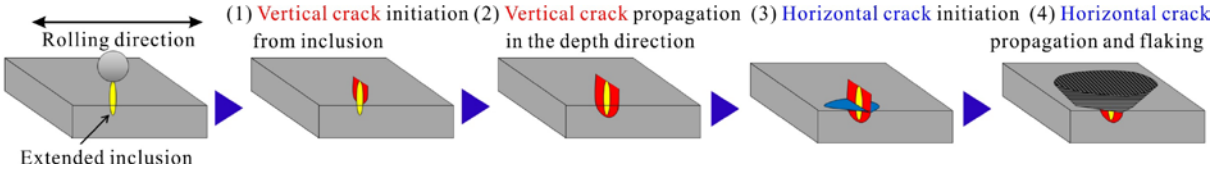

(b) S-type long inclusion.

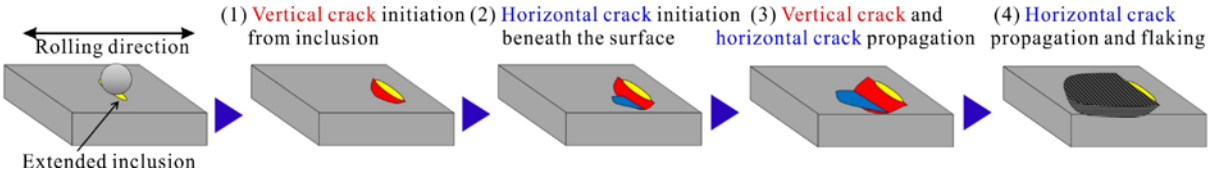

(c) T-type long inclusion.

Figure 12. Models of flaking mechanism from extended inclusion.

Table 1. Fatigue lives of 0.049S mass% material ($N_{i,V}$: Vertical crack initiation, $N_{i,H}$: Horizontal crack initiation, N_f: Flaking).

Material	$N_{i,V}$	$N_{i,H}$	N_f	$N_{i,H}$ - $N_{i,V}$	N_f - $N_{i,H}$
S-type Inclusion (Long)	6.00×10^6	6.80×10^6	7.67×10^6	0.80×10^6	0.87×10^6
	7.50×10^6	8.80×10^6	9.65×10^6	1.30×10^6	0.85×10^6
T-type inclusion	2.50×10^6	2.50×10^6	3.13×10^6	0.00×10^6	0.63×10^6
	1.00×10^6	2.00×10^6	2.95×10^6	1.00×10^6	0.95×10^6